Available online at www.sciencedirect.com
ScienceDirect
International Journal of Heat and Mass Transfer 51 (2008) 4238–4248
International Journal of HEAT and MASS TRANSFER
www.elsevier.com/locate/ijhmt

Experimental study of temperature distribution and local heat flux for turbulent Rayleigh–Bénard convection of air in a long rectangular enclosure

Anna Ebert *, Christian Resagk, André Thess

Ilmenau University of Technology, Department of Mechanical Engineering, P.O. Box 100565, 98684 Ilmenau, Germany

Received 27 July 2007
Available online 24 March 2008

Abstract

Measurements of temperature distribution and local heat flux were performed in a rectangular Rayleigh–Bénard (RB) cell with aspect ratios $\Gamma_x = 5$ and $\Gamma_y = 1$ using air as the working fluid. The range of Rayleigh numbers was from $Ra \approx 6 \times 10^7$ up to $Ra \approx 6 \times 10^8$ and the measurements were taken at four different positions on the cooling and heating plates. The structure of the temperature profiles was analysed with the scaling to the temperature gradient at the wall γ, calculated from both global Nusselt number (γ_{glob}) and the measured local heat flux density q (γ_{loc}). The measured local Nusselt number in the center of Rayleigh–Bénard cell is found to be significantly higher than the global Nusselt number, which was calculated from a heat transfer law, based on asymptotic considerations from Hoelling and Herwig [M. Hoelling, H. Herwig, Asymptotic analysis of heat transfer in turbulent RB-convection, Int. J. Heat Mass Transfer 49 (2006) 1129–1136]. Profiles scaled with γ_{glob} agree very well with the universal asymptotic temperature profile for $Ra \to \infty$. Conversely, profiles scaled with γ_{loc} have another structure. The results clearly show the difference between the temperature profiles from the theoretical model with walls of infinite extend and from the real RB-cell. In contrast to common opinion the structure of the temperature profile was found to consist of three different behaviors. It has been observed for all profiles a linear behavior in the viscous sublayer directly on the wall, a power law in the boundary layer and a logarithmic function in the overlap layer.

Keywords: Rayleigh–Bénard convection; Heat flux; Boundary layer temperature profile; Temperature gradient

1. Introduction

Thermal convection is a frequently occurring type of fluid motion. There is not enough information about the local heat flux and its influence on the temperature distribution in the near wall region and there are just few studies about the relation between the global and local heat flux in a convection cell [2]. In this publication temperature and local heat flux measurements under similar boundary conditions are reported.

The Rayleigh–Bénard experiment is a common model for the study of turbulence and heat transport in thermal convection. Rayleigh–Bénard convection occurs in a fluid between a lower heated plate with the temperature T_{hot} and an upper cooled plate with the temperature T_{cool}. The temperature difference $\Delta T = T_{hot} - T_{cool}$ between both plates drives the flow. The convection cell is adiabatic at the side walls and has isothermal top and bottom plates. This kind of convection can be fully described by five control parameters, namely the Rayleigh number (Ra), the Prandtl number (Pr), the Nusselt number (Nu) and two aspect ratios Γ_x and Γ_y. The Rayleigh and Prandtl numbers are given by

$$Ra = \frac{\beta g \Delta T h^3}{\nu \alpha} \quad \text{and} \quad Pr = \frac{\nu}{\alpha}, \tag{1}$$

whereas the aspect ratios are defined as

* Corresponding author. Tel.: +49 3677691283; fax: +49 3677692441.
E-mail address: anna.ebert@tu-ilmenau.de (A. Ebert).

0017-9310/$ - see front matter © 2008 Elsevier Ltd. All rights reserved.
doi:10.1016/j.ijheatmasstransfer.2008.01.017

Nomenclature

A	parameter of temperature profile
B	parameter of temperature profile
C	parameter of temperature profile
D	parameter of temperature profile
g	gravitational acceleration
h	vertical distance between the plates
l	length of the convection cell
Nu	Nusselt number, $(\partial T/\partial z)\|_{z=0} \cdot h\Delta T$
Q_{12}	radiative heat flux, defined in Eq. (21)
q, q_{rad}	heat flux density, radiative heat flux density
Pr	Prandtl number, ν/α
Ra	Rayleigh number, $\beta g \Delta T h^3/\nu\alpha$
T	mean temperature
T_{cold}, T_{hot}	temperature of the cooling and heating plate
T_{bulk}	temperature in the bulk area, $(T_{\mathrm{cold}} + T_{\mathrm{hot}})/2$
T_{c}	reference temperature, defined in Eq. (5)
ΔT	temperature difference between the plates
x	coordinate parallel to the plates
X_{p}, X_{c}	measurement positions
z	coordinate normal to the plates
z^+	scaled coordinate normal to the plate, defined in Eq. (9)

Greek symbols

α	thermal diffusivity
β	coefficient of thermal expansion
Γ	power law diagnostic function
Γ_x, Γ_y	aspects ratio
γ	temperature gradient at the wall, $\partial T/\partial z\|_{z=0}$
δ	reference length scale, defined in Eq. (6)
ε	emissivity of the plates
Θ^+	normalised temperature, defined in Eq. (8)
ν	kinematic viscosity
Ξ	logarithmic diagnostic function
σ	Stefan–Boltzmann constant, $\sigma = 5.67 \times 10^{-8}$ W/m^2 K^4
φ	view factor of the plates surfaces

$$\Gamma_x = \frac{l}{h} \quad \text{and} \quad \Gamma_y = \frac{w}{h}. \tag{2}$$

The heat flux through the cell is characterised by the Nusselt number defined as

$$Nu = \left.\frac{\partial T}{\partial z}\right|_{z=0} \cdot \frac{h}{\Delta T}. \tag{3}$$

In the given equations the following variables were used: β – coefficient of thermal expansion, g – acceleration of gravity, h – height between heating and cooling plate, l – length of the cell, w – width of the cell, ν – kinematic viscosity, α – thermal diffusivity and $\partial T/\partial z|_{z=0}$ – temperature gradient at the wall.

The transition to the turbulent regime in air occurs when the value of Ra reaches 10^6 [3]. This regime is the focus of the paper, where the Ra range is $6 \times 10^7 < Ra < 6 \times 10^8$. In the present work we use a convection cell with one large aspect ratio, namely $\Gamma_x = 5$, and one intermediate aspect ratio $\Gamma_y = 1$.

The theory behind the Rayleigh–Bénard experiment assumes that the horizontal plates extend infinitely, whereas the heat flux is assumed to be constant for the whole plate surface [1]. Since the total heat flux is a characteristic quantity for RB-convection, it can be used for the analysis of temperature profiles. A new theoretical study of Hoelling and Herwig concerns the asymptotic analysis of the near-wall region of turbulent natural convection [4]. In contrast to the previous studies they tried to find an uniform theory for the temperature profile in the system with horizontal walls of infinite extent. According to Hoelling and Herwig the preliminary quantity to nondimensionalise the temperature profiles is the heat flux density q defined as

$$q = \lambda \cdot \left.\frac{\partial T}{\partial z}\right|_{z=0}. \tag{4}$$

For simplification of the representation of our data we determine the temperature gradient at the wall as $|\partial T/\partial z|_{z=0} = \gamma$.

The natural scale of the temperature variations, a so-called reference temperature T_{c} is an analog to the friction velocity in turbulent shear flows and is composed of the temperature gradient at the plate and material properties of the fluid:

$$T_{\mathrm{c}} = \left(\frac{\alpha\nu}{g\beta} \cdot \gamma^3\right)^{1/4}. \tag{5}$$

With temperature T_{c} the length scale of the boundary layer and the overlap layer can be defined as

$$\delta = \frac{T_{\mathrm{c}}}{\gamma}, \tag{6}$$

true for

$$\lim_{Ra \to \infty} \frac{\delta}{h} = 0. \tag{7}$$

Analogous temperature and length scales have been already used for the study of the thermal convection in the past by Priestley and Townsend [5,6], have been mentioned by Maystrenko et al. [7] and have latterly been successfully applied by Hoelling and Herwig to represent temperature profiles at the vertical heated walls [4] as well as the temperature profiles in RB-convection [1].

The nondimensional temperature Θ^+ is defined via

$$\Theta^+ = \frac{T_{\text{hot}} - T}{T_c} \tag{8}$$

and the nondimensional length z^+ via

$$z^+ = \frac{z}{\delta} = \gamma \cdot \frac{z}{T_c}. \tag{9}$$

Hoelling and Herwig proposed the asymptotical structure of the temperature profile in RB-convection, where for the overlap layer the following logarithmic function is valid:

$$\lim_{z^+ \to \infty} \Theta^+ = C \ln(z^+) + D \tag{10}$$

and for the viscous sublayer the following linear equation is valid:

$$\Theta^+ \sim z^+. \tag{11}$$

This authors analysed experimental and numerical data of many previous studies and hence postulated for the overlap layer an universal temperature profile for $Ra \to \infty$:

$$\Theta^+ = C \ln(z^+) + D, \quad \text{where } C = 0.1,\ D = 3.43. \tag{12}$$

They were unable to found any power law behavior in the curve progression of $\Theta^+(z^+)$.

At the same time many further studies supported the power law scaling in the form

$$\Theta^+ = Bz^{+A} \tag{13}$$

for the temperature in Rayleigh–Bénard convection [7,8] as well as for the mean velocity in pipe and channel flows [9–11].

Not only the vertical distribution of the temperature but also the distribution of the heat flux is an open question of the RB-convection. It was already mentioned that the Nusselt number describes the heat transport through the fluid in the cell. The global Nusselt number as a function of the Rayleigh number has been investigated extensive in the past. Unfortunately, a uniform theory for $Nu = f(Ra, Pr, \Gamma)$ does not exist. One of the first investigations was done by Priestley [5]. He postulated the power law

$$Nu \sim Ra^{1/3}. \tag{14}$$

The later investigations with higher accuracy in helium ($Pr = 1$) of Castaing et al. [12] show another power law

$$Nu \sim Ra^{2/7}. \tag{15}$$

The 2/7-power law was proved in many later experimental and theoretical studies [13–15]. Furthermore, Grossmann and Lohse developed a theory, assuming dissipation in the boundary layer and the mean flow [16]. They composed a phase diagram with different power laws for the different regions of Ra and Pr. In our Ra range ($6 \times 10^7 < Ra < 6 \times 10^8$) and $Pr = 0.7$ the Nusselt number is located in the area $I - l$ and is defined as

$$Nu = 0.27 Ra^{1/4} Pr^{1/8}. \tag{16}$$

Based on their universal profile (12) Hoelling and Herwig proposed a new asymptotic Nu–Ra correlation for $Ra \to \infty$ as an alternative for the theory of Grossmann and Lohse:

$$Nu = \frac{Ra^{1/3}}{\left[\frac{C}{2}\ln\left(\frac{0.078}{16} \cdot Ra^{1.323}\right) + 2D\right]^{4/3}}, \tag{17}$$

$$\text{where } C = 0.1 \quad \text{and} \quad D = -\frac{14.94}{Ra^{0.52} + 3.43}. \tag{18}$$

This Nu–Ra relation defines the global Nusselt number assumed as constant in each point of RB system, which consists of two horizontal plates of infinite extent.

Thereby it is a fact that in a real system with horizontal plates of finite extent, which are bounded by vertical walls, and Rayleigh numbers, that are not yet large enough for the asymptotic representation ($Ra \to \infty$), the local heat flux is distributed over the plate surface in an uneven way. The measurements of Lui and Xia [2] in a water filled cylindrical cell for $10^8 < Ra < 10^{10}$ show, that the local Nusselt number Nu_{loc} in the center of the cell is approximately 20% higher than global Nusselt number Nu_{glob}. Whereas the simple arithmetic average of Nu_{loc} from 11 different positions on the plate becomes very close to Nu_{glob}.

We performed a series of high accuracy temperature and heat flux measurements and as a result we can contribute to the form of the local temperature profile, without influences of any kind of averaging. In this work the scaling of the temperature profiles was done with the theoretical global (index: glob) temperature gradient estimated from Nu_{glob} and measured local (index: loc) temperature gradient estimated from measured heat flux density q. The results of both methods were compared.

To sum up, the main focus of this paper is in the extensive study of the structure of the temperature profiles in the given Ra range and the analysis of the self-similarity of the temperature profiles. Moreover, the difference between the theoretical prediction and the experimental results for the temperature distribution in the RB-cell will be investigated. We are also interested in the heat transport through the cell in a turbulent regime and their dependence on Ra, as well as the difference between local and global Nusselt numbers.

2. Experimental method and procedures

2.1. Experimental setup

In Fig. 1, the configuration of the RB-cell used in the present experiment is shown. The cell is a rectangular box with a 2.5 m length, a 0.5 m width and a 0.5 m height. The working fluid is air. The box is heated from below (cooled from above) by means of 37 mm thick water-heated (water cooled) aluminium plates. The side walls of the cell have a thickness of 8 mm and are made of Perspex. In order to reduce heat losses between the cell and the environment, the side walls are insulated with 180 mm thick Styrodur.

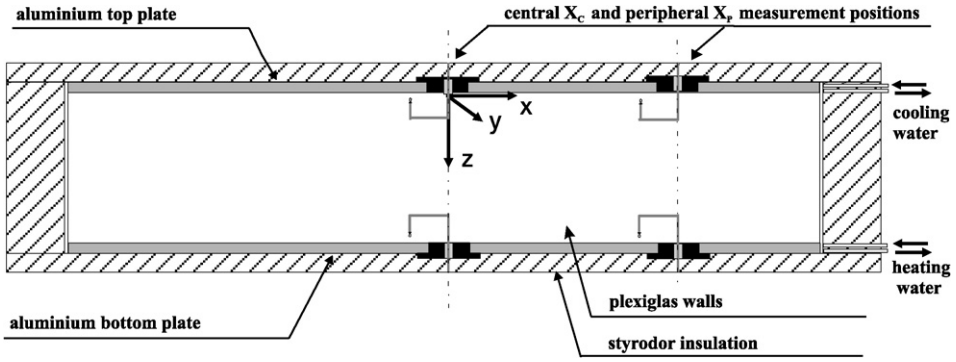

Fig. 1. Schematic of Rayleigh–Bénard cell with central X_c and peripheral X_p measurement positions (cut along the longitudinal axis of the cell).

The so-called sandwich construction of the cooling and heating plates ensures a high temperature distribution homogeneity on the surface of the plates. In the hard aluminium coverage copper pipes with diameter of 20 mm are uniformly placed. Through this pipes the heating or cooling water is streaming. The schematic of the pipe orientation in the plate is shown in Fig. 2a as well as the cross sectional view of such plate is given in Fig. 2b. The distance between the cooper pipes in the plate is only 30 mm. The high volume rate of the water flow and the good thermal conductivity of the aluminium coverage of the plates ensure usually a temperature distribution homogeneity of ± 0.1 K on the surface of the plates. The temperature distribution on the surfaces was monitored by 40 PT-100 temperature probes, which where placed on the longitudinal and lateral axis of the plates and are marked in Fig. 2a with black dots. Both plates where tempered by separate water circulation systems. The heating and cooling apparatus have an accuracy of temperature adjustment of ± 0.1 K. We were able to reach a temperature difference of $\Delta T = 5 \ldots 80$ K between both plates, limited by boiling temperature and dew point of water. Three big measurement windows with a diameter of 100 mm (Fig. 2a) allow the placement of the measuring probes in the convection cell. This windows are permanent closed by aluminium top covers with the wiring of the sensors.

With the described temperature interval from the minimum cooling plate temperature of 10 °C and the maximum heating plate temperature of 90 °C, and with the distance between the plates of $h = 0.5$ m we can cover a range of Rayleigh numbers from 6×10^7 up to 6×10^8. Our Cartesian coordinate system was defined as follows. We located the origin at the center of the lower surface of the cooling plate. The x-axis is parallel to the long side of the upper plate, and the z-axis is oriented downward. We were able to do the local temperature measurements at three measurement windows, respectively on the heating and the cooling plate. We used the windows in the center of the plates as the central measurement position (index: c). Due to the symmetrical structure of the large-scale convection flow, described in [7], just one of two peripheral measurement position was used for the measurement (index: p). Regarding the construction of the sensor support x-coordinate $X_c = -65$ mm for the central measurement position

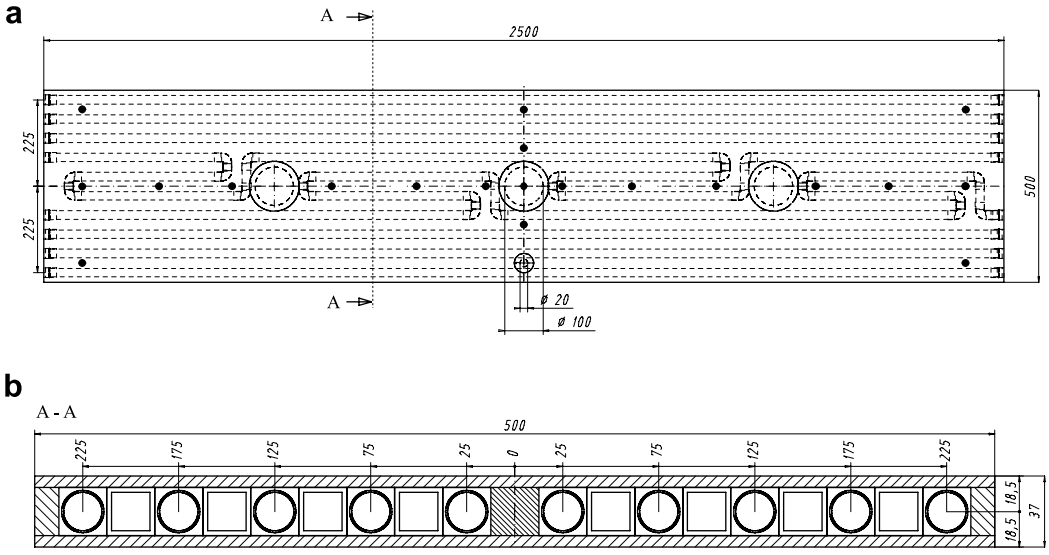

Fig. 2. Construction of the plates (a) and their cross sectional view (b).

and x-coordinate $X_p = 585$ mm for the peripheral measurement positions were relevant (Fig. 1).

2.2. Measurement system

For the temperature measurement two sensor systems based on glass-encapsuled NTC microthermistors with a diameter of 120 μm have been used. Each thermistor have been mounted on a 4 mm thick support (Fig. 3). The sensors can be moved up to $z = 150$ mm distance from cooling and heating plates simultaneously with two 1D traverse systems with a smallest step of 10 μm. A personal computer operates automatically the step motor of the traverse systems. The minimal distance between sensor and plate corresponds to the half of the thermistor diameter.

A very low current has been used for the thermistor operation in order to avoid measurement errors due to a self-heating effect. For the amplification of the resistance variance of the thermistor a resistance bridge with an internal DC voltage source has been used. This bridge reconverts the resistance variance of the thermistor to a voltage signal and amplifies this signal by a factor of 100. The output voltage of the bridge is measured by a digital multimeter Agilent 34970A with an integrated 349020A 16-Channel-Reed-Multiplexer. We used two channels with a sampling rate of 66 Hz, resulting in 33 Hz for each of the two channels. The personal computer converts the voltage signal to the temperature values by means of the calibration curves, which were unique for each microthermistor.

The measurement interval is located between $0.07\text{ mm} < z < 150\text{ mm}$ distance from the cooling and heating plates and is sampled at 68 non-equidistant positions with 10 μm steps in the vicinity of the plates, resulting in two simultaneously measured temperature profiles with 34 z-positions each one. The measuring time for each position was approximately 1 h, resulting in $k \approx 119,000$ temperature values for one position. In other words 68 temperature series $T_i(z)$ with $1 \leqslant i \leqslant k$ represent the raw data for two simultaneously measured temperature profiles.

After the completion of the temperature measurements the heat flux measurements were performed under exactly the same boundary conditions. The measurement was done with commercial heat flux sensors Ahlborn, model 120. The sensors have a diameter of 33 mm and thickness of 1.5 mm and are made from epoxy resin. We placed four heat flux sensors in the cell on the surface of the heating and cooling plates at X_c and X_p (Fig. 1a and b). For each temperature profile, the heat flux density at the plate was measured. The accuracy of the sensors was given as 5% at 25 °C by the manufacturer. A laboratory assay showed for temperature $T = 20\,^{\circ}\text{C}$ a dispersion of ±5%, for $T = 50\,^{\circ}\text{C}$, ± 7% and for $T = 80\,^{\circ}\text{C}$, ± 10%. These values will be used for the estimation of the deviation of the heat flux measurements.

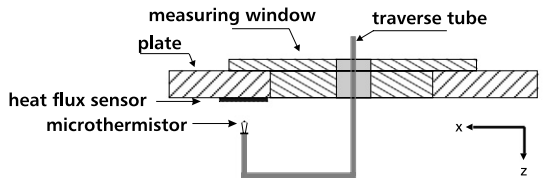

Fig. 3. Schematic of the thermistor probe positioning for both measurement positions.

3. Experimental results

3.1. Temperature profiles

We performed measurements of temperature time series $T_i(z)$ and local heat flux density q at both positions X_c and X_p at the heating and cooling plate. At both positions the temperature was measured simultaneously with the same distance from the cooling and heating plate. The measurements were carried out for seven Rayleigh numbers, summarised in Table 1. From the temperature time series $T_i(z)$ the temperature profiles were calculated by

$$T(z) = \frac{1}{K}\sum_{i=1}^{K} T_i(z). \tag{19}$$

The overview of six temperature profiles measured at X_p is given in Fig. 4. We found typical boundary layer profiles, the temperature grows very fast near the heating and cooling plate and is constant in the bulk. The profiles measured on the heating and cooling plate are nearly symmetrical and at the distance of $z = 150$ mm always already reach the bulk temperature T_{bulk}. We can assume, that the temperature remains constant for the 200 mm – intermediate bulk area. In the inset of Fig. 4 the absolute measurement errors for the highest Ra ($Ra = 6 \times 10^8$) and the lowest Ra

Table 1
Complete set of Rayleigh numbers, temperatures of cooling (T_{cool}) and heating (T_{hot}) plate at which the temperature profiles and the local heat flux density q were measured, as well as the measured heat flux densities on the cooling plate (q_{cool}) and the heating plate (q_{hot}) and the calculated radiative heat flux densities q_{rad}

Position	Ra	T_{plate} (°C)		q (W/m^2)		q_{rad} (W/m^2)
		T_{cool}	T_{hot}	q_{cool}	q_{hot}	
X_c	6.02×10^8	12.91	87.13	462.42	441.76	25.75
	4.10×10^8	14.95	56.10	229.52	205.66	12.33
	2.79×10^8	15.94	41.12	129.98	113.53	7.02
	1.92×10^8	15.96	32.07	68.62	76.49	4.36
	1.30×10^8	17.09	27.73	42.62	47.87	2.79
	8.91×10^7	16.92	24.00	25.69	31.83	1.82
	6.16×10^7	17.29	22.12	18.33	19.16	1.23
X_p	6.00×10^8	12.90	87.18	411.11	503.47	25.77
	4.10×10^8	15.00	56.08	203.17	227.95	12.31
	2.79×10^8	15.91	41.11	115.72	125.69	7.03
	2.00×10^8	15.90	32.70	81.58	74.94	4.49
	1.30×10^8	17.10	27.79	49.62	43.80	2.80
	8.89×10^7	16.93	23.99	28.65	28.10	1.81
	6.16×10^7	17.23	22.08	20.196	17.91	1.23

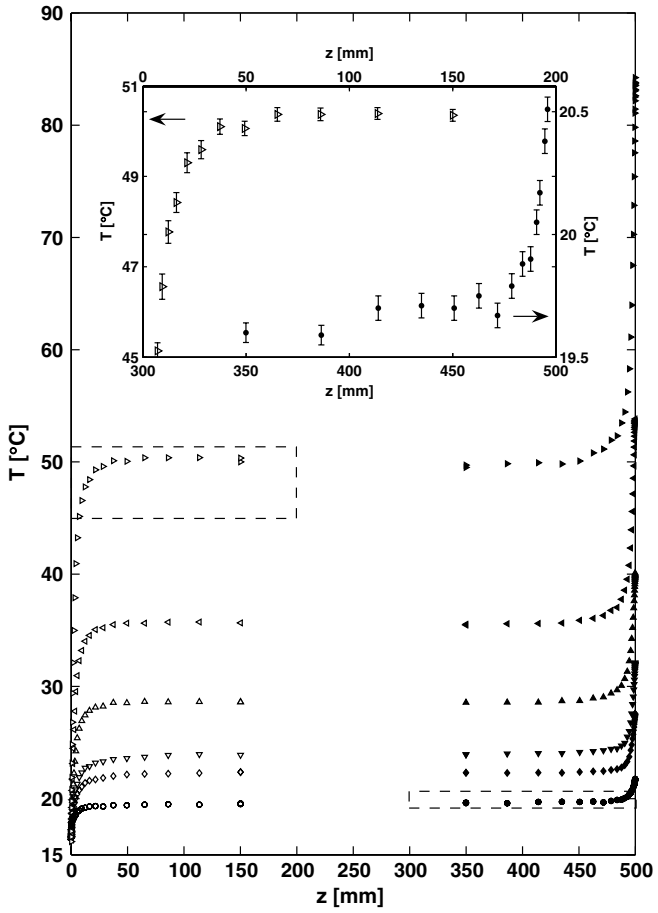

Fig. 4. Simultaneously measured temperature profiles $T(z)$ at the position X_p: $Ra = 6.2 \times 10^7$ (•), $Ra = 1.3 \times 10^8$ (◆), $Ra = 2 \times 10^8$ (▼), $Ra = 2.79 \times 10^8$ (▲), $Ra = 4.1 \times 10^8$ (◀), $Ra = 6 \times 10^8$ (▶) for $T(z)$ measured at the heating plate; the same empty symbols apply for the measurements at the cooling plate. The inset shows a zooming of $T(z)$ for $Ra = 6.2 \times 10^7$ and $Ra = 6 \times 10^8$ with error bars.

$(Ra = 6.2 \times 10^7)$ have been indicated by error bars. The measurement uncertainty consists on the systematical uncertainty and precision limit, which is defined as confidence interval for 95% of all measured temperature values. The relative measurement uncertainty increases with decreasing Rayleigh number. It is less than 1% for $Ra = 6 \times 10^8$ and less than 2.5% for $Ra = 6 \times 10^7$.

In our previous work [7] we were not able to represent the temperature profiles in wall variables, because of the absence of information about heat flux. In present work we normalised our profiles as recommended by Hoelling and Herwig [1]. Due to our convection cell having a large aspect ratio of $\Gamma_x = l/h = 5$, the boundary conditions are approximately comparable to the theoretical case with the walls of infinite extent.

It should be mentioned, that in [1] the temperature profiles were analysed with temperature gradient γ obtained from the analytical Nu–Ra dependency (17). Whereas the global Nusselt number Nu_{glob} presents the average of heat flux over the whole plate surface. According to this, the temperature gradient $\gamma(Nu_{glob})$ shows the average of temperature gradients over the whole plate. The real distribution of the heat flux on the plate surface is uneven and impacts the vertical temperature distribution in the cell. In other words, the theoretical temperature gradient estimated from the global heat flux $\gamma(Nu_{glob})$ could be different from the local temperature profile near the wall.

In conclusion, the measurement of the local heat flux density q is needed for the calculation of γ, in order to get the non-averaged local temperature profile. Hence the variations of the local heat flux will be included in the temperature gradient $\gamma(q)$ and in the normalised temperature profile $\Theta^+(z^+)$.

3.2. Heat transfer

One of the most frequently discussed questions in RB-convection concerns the heat transfer through the fluid layer. At positions X_c and X_p local heat flux density q on the cooling plate q_{cool} and the heating plate q_{hot} was measured simultaneously. The results are summarised in Table 1. From q we calculated local Nusselt numbers by

$$Nu_{loc} = \frac{q}{\lambda} \cdot \frac{h}{\Delta T}. \tag{20}$$

We did not have the possibility to determine the global heat flux in the cell experimentally. Thus we used the theoretical predictions of [1,16] and calculated the global Nusselt number Nu_{glob} according to (16) and (17).

The results are compared in Fig. 5 and Table 2. First of all we see a large difference between Nu_{loc} and Nu_{glob}. The local heat flux along the longitudinal axis of the cell appears to be more than 50% higher than the global heat flux. Also the differences between Nu_{loc} at different positions is quite visible. However, these fluctuations are small enough to be caused by measurement errors. They are shown in Fig. 5 with error bars.

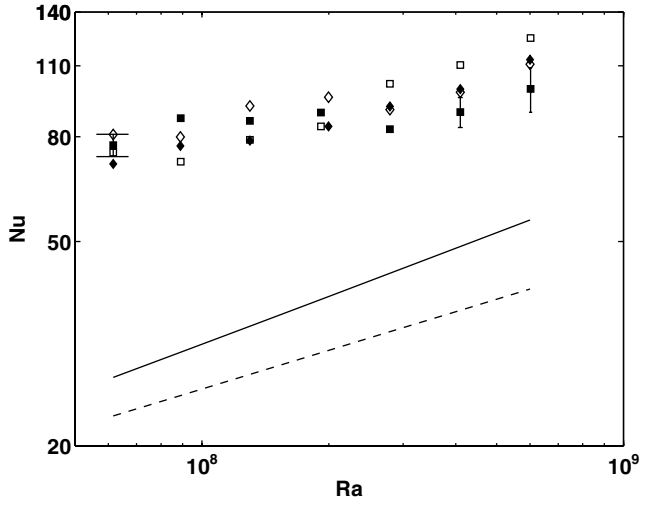

Fig. 5. Comparison of global Nu calculated from analytical Nu–Ra dependencies (16) (dotted line) and (17) (solid line); local Nu measured at position X_c on the cooling plate (□) and the heating plate (■) and at position X_p on the cooling plate (◇) and the heating plate (◆).

Table 2
Complete set of Nusselt numbers: Nu_{loc} measured on the cooling and heating plates and Nu_{glob} calculated from analytical dependencies (17) and (16), as well as the local temperature gradients γ_{loc} calculated from q and the global temperature gradients γ_{glob} calculated from Nu_{glob} (17)

Position	Ra	Nu_{loc}		Nu_{glob}		γ_{loc} (K/m)		γ_{glob} (K/m)
		Heating plate	Cooling plate	(17)	(16)	Heating plate	Cooling plate	(17)
X_c	6.02×10^8	124.57	99.17	55.14	40.43	18,497	14,725	8185
	4.10×10^8	110.39	89.38	48.89	36.73	9072	7345	4024
	2.79×10^8	101.49	82.78	43.37	33.37	5117	4174	2184
	1.92×10^8	83.80	89.19	38.57	30.37	2702	2876	1243
	1.30×10^8	78.91	85.94	34.20	27.56	1671	1820	728
	8.91×10^7	71.55	86.95	30.44	25.08	1007	1224	431
	6.16×10^7	74.57	77.04	27.18	22.87	719	743	263
X_p	6.00×10^8	110.75	113.03	55.10	40.40	16,444	16,782	8184
	4.10×10^8	97.72	99.06	48.89	36.73	8030	8141	4017
	2.79×10^8	90.36	91.65	43.37	33.37	4556	4621	2186
	2.00×10^8	95.53	83.80	39.07	30.68	3212	2817	1313
	1.30×10^8	91.87	78.63	34.20	27.56	1945	1665	731
	8.89×10^7	79.95	76.76	30.42	25.06	1126	1081	430
	6.16×10^7	80.82	70.84	27.18	22.87	792	694	264

As showed by Lui and Xia [2] Nu_{glob} displays the average of Nu_{loc} over the plate surface. Furthermore, they found Nu_{loc} in the center of cylindrical cell is approximately 20% higher than Nu_{glob}. The same significant differences between Nu_{loc} and Nu_{glob} were observed by du Puits et al. in a large-scale cylindrical convection cell, whose results will be published in the future [17]. This results of [2,17] support our data.

3.3. Radiation exchange

Nu_{glob} was calculated by Eqs. (16) and (17) without considering the influence of radiation. Due to of emission and absorption between two surfaces with different temperatures a heat flux caused by the radiation exists. One could imagine, that this radiative heat flux influences the measurement data of q_{cool} and q_{hot} and could be the cause of $Nu_{loc} \neq Nu_{glob}$.

For the radiation exchange between two diffuse gray surfaces under consideration of reflections is given [18]:

$$Q_{12} = \frac{\sigma \varepsilon_1 \varepsilon_2 A_1 \varphi_{12} (T_{hot}^4 - T_{cool}^4)}{1 - (1-\varepsilon_1)(1-\varepsilon_2)\varphi_{12}\varphi_{21}}, \tag{21}$$

whereas $\sigma = 5.67 \times 10^{-8}\ \mathrm{W/m^2\,K^4}$ – the Stefan–Boltzmann constant, ε_1 and ε_2 – the emissivities, φ_{12} and φ_{21} – the view factors of the surfaces are.

This equation was used to determine the radiation exchange between the heating plate and the heat flux sensor fixed on the cooling plate as well as between the cooling plate and the heat flux sensor fixed on the heating plate. The heat flux sensors have a surface area of $A_2 = 3.14 \times 10^{-4}\ \mathrm{m^2}$, a emissivity of $\varepsilon_2 = 0.9$ (plastic material) and a view factor of $\varphi_{21} = 1$. The heating and cooling plates have surface areas of $A_1 = 1.25\ \mathrm{m^2}$, a emissivity of $\varepsilon_1 = 0.05$ (polished aluminium) and a view factor of $\varphi_{12} = \varphi_{21}\frac{A_2}{A_1} = 2.5 \times 10^{-4}$.

The in that way calculated radiative heat flux density $q_{rad} = Q_{12}/A_2$ is also summarised in Table 1. We can see, that the radiation exchange is always present, but the radiative heat flux density q_{rad} represents only 5–7% of the measured q_{cool} and q_{hot}.

It can be summarised, that the influence of the radiation exchange is to small to cause the 50% difference between Nu_{loc} and Nu_{glob}.

3.4. Temperature gradient

Since the local heat flux is much larger than the theoretical global heat flux, the temperature gradient calculated from the measured heat flux density γ_{loc} is much higher than the gradient calculated from the theoretical Nu–Ra prediction (17) γ_{glob}:

$$\gamma_{loc} = \frac{q}{\lambda}; \quad \gamma_{glob} = \frac{Nu_{glob} \cdot \Delta T}{h}. \tag{22}$$

For all temperature profiles the local temperature gradient γ_{loc} calculated from q and global temperature gradient γ_{glob} calculated from Nu_{glob} are also summarised in Table 2.

An example of the temperature profile, measured by $Ra = 8.8 \times 10^7$ at the cooling plate (X_c) is shown in Fig. 6. It is quite evident that the measured local gradient conforms much better with the temperature profile than the global theoretical gradient. This example is typical for all measured data. We can conclude that γ_{glob}, which is basically an averaged temperature gradient for the whole plate surface, is not representative for the local temperature profiles. Consequentially, γ_{glob} should not be used to analyse the measured temperature profiles because the local gradient variations are not taken in account.

4. Analysis

4.1. Structure of the temperature profiles

We normalised our profiles for the cooling plate Θ_c^+ and for the heating plate Θ_h^+ via

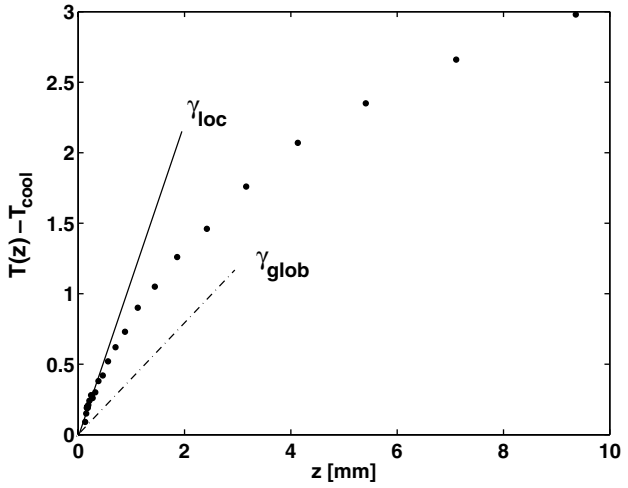

Fig. 6. Near wall part of the temperature profile (•) ($Ra = 8.8 \times 10^7$) compared with measured γ_{loc} and theoretical γ_{glob} temperature gradients.

$$\Theta_c^+ = \frac{T(\delta z^+) - T_{cool}}{T_c}, \quad \Theta_h^+ = \frac{T_{hot} - T(\delta z^+)}{T_c}. \tag{23}$$

The distance z was normalised as per Eq. (9):

$$z^+ = \frac{z}{\delta} = \gamma \cdot \frac{z}{T_c}. \tag{24}$$

We calculated the reference temperature T_c (5) twice, with theoretical γ_{glob} and measured γ_{loc} temperature gradients. As expected, the differences between γ_{glob} and γ_{loc} cause great differences in the curve structure of the normalised profiles $\Theta^+(z^+)$. In Fig. 7 an example for $Ra = 1.9 \times 10^8$ measured at the cooling plate (X_p) is shown. The profile normalised to γ_{glob} corresponds very well to examples of normalised profiles from Hoelling and Herwig [1]. The same profile normalised to γ_{loc} has another structure. This difference, systematical for all analysed temperature profiles, will be discussed later.

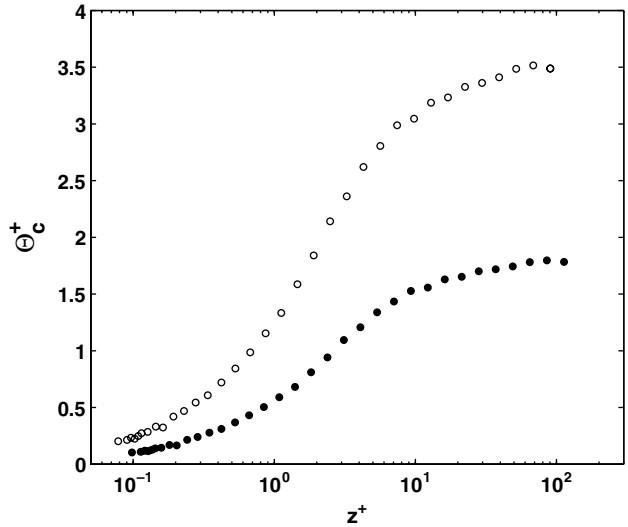

Fig. 7. Temperature profile $\Theta_c^+(z^+)$ measured at $Ra = 1.9 \times 10^8$ (X_c) and normalised with γ_{glob} (○) and γ_{loc} (●).

The next important property is the structure of the temperature profiles in the near wall region. The complete set of temperature profiles measured at the central measurement position X_c and normalised to γ_{loc} in semi-logarithmic (Fig. 8a) and double-logarithmic (Fig. 8b) representations are shown. By comparison with examples of measured profiles used in [1], our data demonstrates a significantly higher spatial and temporal resolution. For clear representation the profiles have been shifted by a factor of +2 (Fig. 8a) and a factor of ×10 (Fig. 8b).

Three areas with different behaviors of $\Theta^+(z^+)$ were found for all temperature profiles. They are separated with dotted lines and colored gray in Fig. 8. At first for the viscous sublayer directly on the plate ($z^+ < 0.2$) a linear dependency $\Theta^+ = az^+ + b$ similar to (11) has been obtained. However, this area, separated in Fig. 8a with the first dotted line, is much thinner than in examples from [1], in which the profile is linear up to $z^+ \approx 2$.

In the next step the logarithmic region could be confirmed with our data. This region is located far from the wall in the so-called overlap layer. In this area $8 < z^+ < 100$ a logarithmic behavior $\Theta^+ = C\ln(z^+) + D$ (10) was observed. This area is also separated in Fig. 8a with dotted lines and colored gray, the data are approximated with solid lines.

In contrast to Hoelling and Herwig [1] a wide region with a distinct power law behavior between linear and logarithmic areas was observed. In a double-logarithmic representation (Fig. 8b) the approximation of this grey colored area with $\Theta^+ = Bz^{+A}$ for $0.2 < z^+ < 3$ are shown with solid lines. The aberration of the temperature profiles and linear behavior, proposed by Hoelling and Herwig [1] for this region, can be obtained from Fig. 8a. In our previous publication we already observed and analysed a power law behavior in the boundary layer [7]. Furthermore, other new experimental studies exist, which indicate the power law behavior [8,19] for temperature and velocity profiles in the near wall layer. A lower spatial resolution of measurements used by Hoelling and Herwig ([1] (Fig. 3)) can be a possible reason why the power law region could not be found.

To prove the power and logarithmic manner the diagnostic function recently suggested by Wosnik et al. [20] was utilised

$$\Xi = z^+\left[\frac{d\Theta^+}{dz^+}\right], \quad \Gamma = \left(\frac{z^+}{\Theta^+}\right)\left[\frac{d\Theta^+}{dz^+}\right]. \tag{25}$$

In Fig. 8c, the logarithmic diagnostic function Ξ shows an approximately constant behavior for $8 < z^+ < 100$, which proposes the logarithm of $\Theta^+(z^+)$. In Fig. 8d, the power law diagnostic function Γ is shown, its constant behavior for $0.2 < z^+ < 3$ verifies the power law.

4.2. Self-similarity of the temperature profiles

We measured the temperature at the heating and cooling plate for seven Ra at both positions X_c and X_p (Table 1),

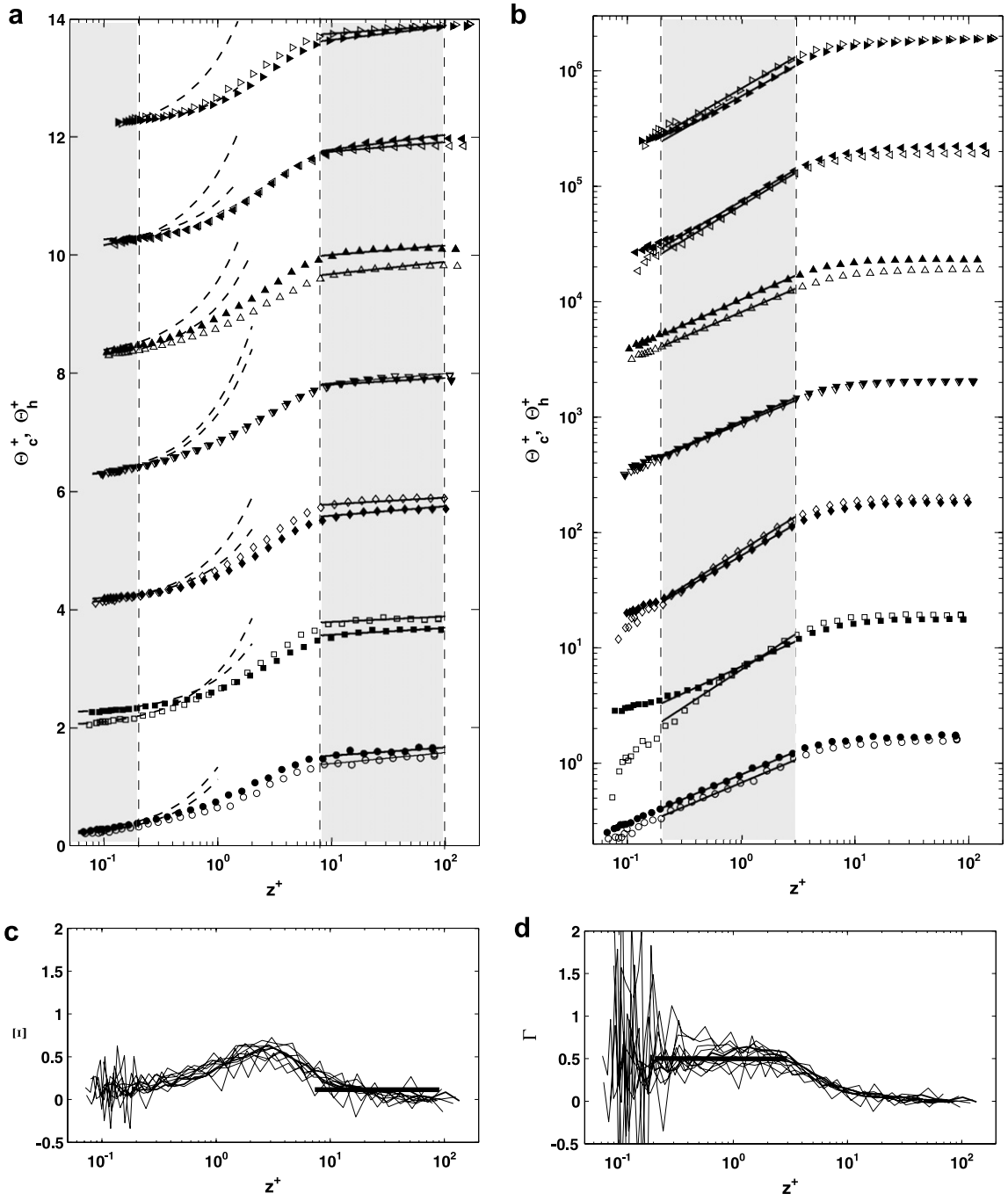

Fig. 8. Normalised temperature profiles, measured at the position X_c at the heating plate: $Ra = 6.16 \times 10^7$ (●), $Ra = 8.91 \times 10^7$ (■), $Ra = 1.3 \times 10^8$ (◆), $Ra = 1.92 \times 10^8$ (▼), $Ra = 2.79 \times 10^8$ (▲), $Ra = 4.1 \times 10^8$ (◀), $Ra = 6.02 \times 10^8$ (▶); the same empty symbols apply for the measurements at the cooling plate. Results are shown in semi-logarithmic (a) and double-logarithmic (b) representations (the areas of linear and logarithmic (a) as well as power (b) manners are colored gray). Logarithmic diagnostic function Ξ (c) and power law diagnostic function Γ (d) calculated for in (a) and (b) shown temperature profiles.

resulting in 28 temperature profiles. They were scaled with γ_{glob} and γ_{loc}.

In both cases we regard the effect of the variable thermal diffusivity coefficient α. It was done by multiplying γ by ratio $\alpha_{wall}/\alpha_{bulk}$, which is the ratio of the thermal diffusivity at wall temperature to thermal diffusivity at bulk temperature. This aspect is especially important for the profiles measured at high Ra, because of the variability of the physical properties of air at a large ΔT.

In this section our analysis will be summarised with a comparison of curve structures at both normalisation. In Fig. 9a and b, the coefficients of approximations with power law $\Theta^+ = Bz^{+A}$ and logarithmic function $\Theta^+ = C\ln(z^+) + D$ are displayed. These coefficients A, B,

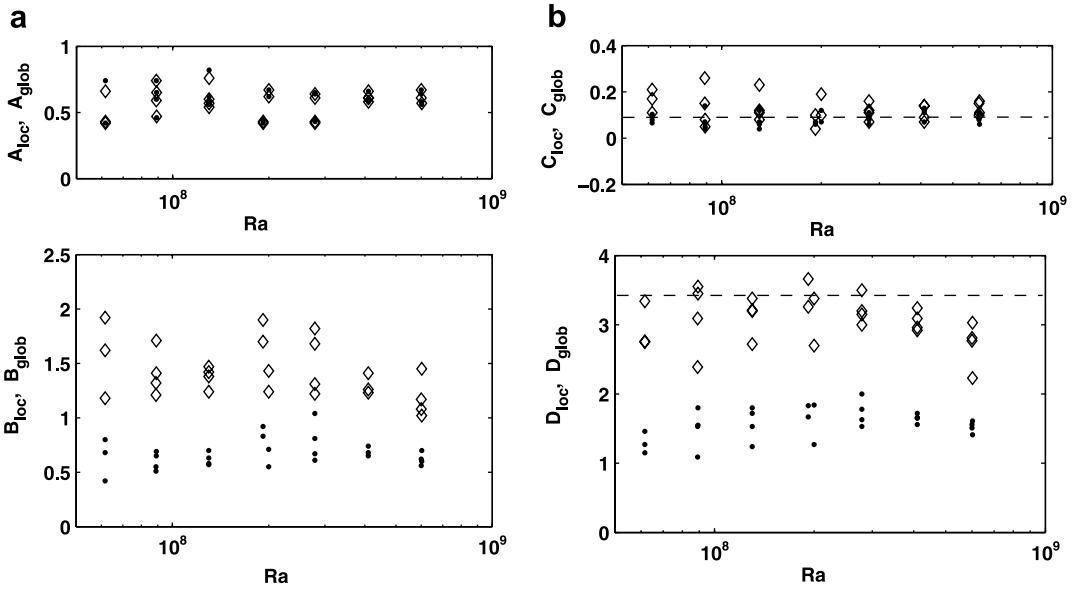

Fig. 9. The coefficients of approximation with $\Theta^+ = Bz^{+A}$(a) and $\Theta^+ = C\ln(z^+) + D$ (b) for temperature profiles normalised with γ_{glob} (◇) resulting in A_{glob}, B_{glob}, C_{glob} and D_{glob}; as well as normalised with γ_{loc} (●) resulting in A_{loc}, B_{loc}, C_{loc} and D_{loc}. Asymptotic values of $C = 0.1$ and $D = 3.43$ are shown with dotted lines.

C and D, obtained from normalisation with γ_{glob} (index: glob) and with γ_{loc} (index: loc), are the focus of our interest.

At first the power law region $\Theta^+ = Bz^{+A}$ at $0.2 < z^+ < 3$ will be discussed (Fig. 9a). The exponent A characterises the slope of the temperature profile. The difference between temperature gradients at the wall γ_{glob} and γ_{loc} impacts slightly on the slope. It varies in the whole Ra range approximately in the interval $0.5 \leqslant A_{loc}, A_{glob} \leqslant 0.7$, without any dependency on Ra. The additive coefficient B is quite affected from the difference between temperature gradients, as expected $B_{glob} > B_{loc}$.

The results of the approximation of the logarithmic region $8 < z^+ < 100$ with $\Theta^+ = C\ln(z^+) + D$ are shown in Fig. 9b. The constant C, characterising the slope, is analogous to $1/\kappa$ from the well known Karman–Prandtl universal log-law. The slope of our profiles C_{loc} conforms well with the theoretical prediction for $Ra \to \infty$ of $C = 0.1$ (dotted line). It is noticeable that C_{glob} deviates from the value of $C = 0.1$ more than C_{loc}. The additive constant D_{glob} fluctuates in a wide interval, but agrees very well with examples from [1]. Here the asymptotic value for $Ra \to \infty$, $D = 3.43$ is also marked with a dotted line. As expected, D_{loc} is much smaller than D_{glob}. We can summarise the results as $D_{loc} = 1.5 \pm 0.5$.

Because of the small Ra range we cannot interpolate the asymptotical values from the parameters A, B, C, D for $Ra \to \infty$. But, due to the Ra-independent fluctuations of this coefficients we can average the approximations of 28 temperature profiles, which have been measured in the middle area of the convection cell. The averaged local coefficients A_{loc}, B_{loc}, C_{loc} and D_{loc} provide following power and logarithmic functions:

$$\Theta^+ = 0.67z^{+0.56} \quad \text{for } 0.2 < z^+ < 3, \tag{26}$$

$$\Theta^+ = 0.09\ln(z^+) + 1.57 \quad \text{for } 8 < z^+ < 100. \tag{27}$$

The results given in Fig. 9 clearly show the difference between the theoretical model with walls of infinite extend and a real RB-cell. The theory basically shows an averaged temperature profile over the whole plate surface. But after accomplishing heat flux measurements, we can assume that the heat flux in the central area of the cell is much higher than the average. Consequently, the temperature profiles normalised to γ_{glob} inevitably have an averaged curve progression. We can summarise that in order to define the local and uninfluenced structure of the temperature profile, the local temperature gradient γ_{loc} has to be used for normalisation.

5. Conclusions

We have studied the mean temperature profiles and local heat flux in turbulent Rayleigh–Bénard convection. The local heat flux was found to be uneven distributed over the plate surface. The temperature gradient at the wall was obtained from the analytical global Nu_{glob} and the measured local Nu_{loc} heat fluxes, and it was decided that the theoretical global temperature gradient γ_{glob} does not conform to the measured temperature profiles. Since the wall temperature gradient is a crucial parameter for analysis, the structure of the normalised temperature profile is directly dependent on this. In order to consider the local variations of the heat flux the local temperature gradients γ_{loc} have to be used for the scaling of the temperature profiles. The outcome is, that the universal temperature profile resulting from asymptotical analysis of the system with walls of infinite extend can not be applied unconditionally in a real RB-cell.

The high resolution of our measurement data enables the extensive analysis of the structure of the temperature

profile. It has been observed for the first time, that three different behaviors in the temperature profile were proved: linear in the viscous sublayer directly at the wall, power law in the boundary layer and logarithmic in the overlap layer between the boundary layer and bulk.

Acknowledgement

The authors thank the Helmholtz Association of German Research Centers for financial support. The work has been also partially supported by the Deutsche Forschungsgemeindschaft (Grant No. TH 497/24-1). We are grateful to R. du Puits, C. Wagner, H. Herwig and M. Hoelling for helpful discussions and to V. Mitschunas and H. Hoppe for their technical support.

References

[1] M. Hoelling, H. Herwig, Asymptotic analysis of heat transfer in turbulent Rayleigh–Bénard convection, Int. J. Heat Mass Transfer 49 (2006) 1129–1136.
[2] S.-L. Lui, K.-Q. Xia, Spatial structure of the thermal boundary layer in turbulent convection, Phys. Rev. E 57 (1998) 5494–5503.
[3] R. Krishnamurti, On the transition to turbulent convection. Part 1, 2, J. Fluid Mech. 42 (1970) 295–320.
[4] M. Hoelling, H. Herwig, Asymptotic analysis of the near-wall region of turbulent natural convection flows, J. Fluid Mech. 541 (2005) 383–397.
[5] C.H.B. Priestley, Convection from a large horizontal surface, Aust. J. Phys. 7 (1954) 176–201.
[6] A.A. Townsend, Temperature fluctuations over a heated horizontal surface, J. Fluid Mech. 5 (1958) 209–241.
[7] A. Maystrenko, C. Resagk, A. Thess, Structure of thermal boundary layer for turbulent Rayleigh–Bénard convection of air in a long rectangular enclosure, Phys. Rev. E 75 (2007) 066303.
[8] R. du Puits, C. Resagk, A. Thess, Structure of thermal boundary layers in turbulent Rayleigh–Bénard convection, J. Fluid Mech. 572 (2007) 231–254.
[9] G.I. Barenblatt, Scaling laws for fully developed turbulent shear flows: Part 1. Basic hypothesis and analysis, J. Fluid Mech. 248 (1993) 513–520.
[10] E.-S. Zanoun, F. Durst, H. Nagib, Evaluating the law of the wall in two-dimensional fully developed turbulent channel flows, Phys. Fluids 15 (2003) 3079–3089.
[11] M.H. Buschmann, M. Gad-el-Hak, Comment on "Evaluating the law of the wall in two-dimensional fully developed turbulent channel flows" [Phys. Fluids 15 (2003) 3079], Phys. Fluids 16 (2004) 3507–3508.
[12] B. Castaing, G. Gunaratne, F. Heslot, L. Kadanoff, A. Libchaber, S. Thomae, X.-Z. Wu, S. Zaleski, G.-M. Zanetti, Scaling of hard thermal turbulence in Rayleigh–Bénard convection, J. Fluid Mech. 204 (1989) 1–30.
[13] B.I. Shraiman, E.D. Siggia, Heat transport in high-Rayleigh-number convection, Phys. Rev. A 42 (1990) 3650–3653.
[14] X.-Z. Wu, A. Libchaber, Scaling relations in thermal turbulence: the aspect ratio dependence, Phys. Rev. A 45 (1992) 842–845.
[15] R. Kerr, Rayleigh number scaling in numerical convection, J. Fluid Mech. 310 (1996) 139–179.
[16] S. Grossmann, D. Lohse, Scaling in thermal convection: a unifying theory, J. Fluid Mech. 407 (2000) 27–56.
[17] R. du Puits, C. Resagk, A. Thess, personal communication.
[18] VDI Verein Deutscher Ingenieure, VDI-Waermeatlas, eighth ed., Springer-Verlag, Berlin, Heidelberg, 1997, pp. Ka1–Ka10.
[19] E.-S. Zanoun, F. Durst, H. Nagib, Scaling laws for turbulent channel and pipe flows over a wide range of Reynolds numbers, in: Proceedings of the Fourth International Conference on Heat Transfer, Fluid Mechanics and Thermodynamics, Cairo, 2005, ZE2.
[20] M. Wosnik, L. Castillo, W. George, A theory for turbulent pipe and channel flows, J. Fluid Mech. 241 (2000) 115–145.